Parametrization of the differential die-away self-interrogation early die-away time for PWR spent fuel assemblies

Li Caldeira Balkeståhl, Zsolt Elter, Sophie Grape
Uppsala University, Division of Applied Nuclear Physics, Uppsala, Sweden

Abstract:

The differential die-away self-interrogation (DDSI) instrument developed and built in Los Alamos National Laboratory (LANL) is being considered for verification before final disposal. One of the signals from this instrument, the early die-away time, has been shown to be proportional to the multiplication of the spent fuel assembly. Full-scale simulations of the instrument response using MCNP are time consuming. This may become a problem in cases when the instrument response to a large number of fuel assemblies is required, such as in the case of training machine learning models.

In this paper, we propose a parametrization of the early die-away time as a function of initial enrichment (IE), burn-up (BU) and cooling time (CT), for intact PWR spent fuel assemblies. The parametrization is calculated from a dataset of 1040 simulated PWR spent fuel assemblies with fuel parameters in the range of IE=2-5%, BU=15-60 GWd/tU and CT=5-70 years. The simulations are done using Serpent2 for the depletion calculation and MCNP6 for the neutron transport and detection in the DDSI.

It was found that the CT dependence can be decoupled from the BU and IE dependence, and that it follows an exponential decay. The BU and IE dependences have been fitted with several different functions, and the best fit was chosen based on the chi-square value. The determination of the die-away time using the parametrization has been tested on a separate dataset, resulting in a root mean square error (RMSE) of 0.6 μs (the early die-away time ranges from 28 μs to 84 μs). A description of this work is given in the paper together with details on the choice of parametrizing function, and qualitative arguments for that choice.

Keywords: DDSI; die-away time; parametrization; modelling; PWR

1. Introduction

The differential die-away self-interrogation (DDSI) technique has been studied by Los Alamos National Laboratory (LANL) [1] as part of the Next Generation Safeguards Initiative - Spent Fuel [2]. A prototype instrument has been manufactured and recently tested on spent nuclear fuel at Clab [3]; the technique may also be considered for future use at encapsulation facilities.

As has been shown in [4] for simulation space, and in [3] and [5] for experimental data, the DDSI early die-away time, τ, is proportional to the multiplication of a fuel assembly. The early die-away time is defined as the decay constant in an exponential fit to the real coincidence Rossi-alpha distribution for neutrons, in the time domain of 4 to 52 μs. The proportionality to the multiplication makes τ an interesting instrument response to study, especially in the context of nuclear safeguards verification where the fuel assembly parameters initial enrichment (IE), burnup (BU) and cooling time (IE) as well as fissile mass are central concepts. The reason is that assembly multiplication reflects the balance between the fissile content and neutron absorbers such as fission products and minor actinides in the assembly. This balance, in turn, varies with the fuel parameters IE, BU, and CT.

Full-scale simulations of the DDSI instrument response using Monte Carlo techniques are however time consuming, especially if many such simulations are needed. For this reason, we here present a parametrization of the early die-away time, as a function of fuel parameters CT, IE and BU, which can be used as an approximation of the instrument response in place of the full simulations.

Section 2 of this paper describes the simulation methods used to obtain the instrument response, section 3 explains how the parametrization was derived and section 4 shows the results of the parametrization for a separate data set.

2. Simulation methods

The simulations of the response of the DDSI instrument to spent nuclear fuel are done in two steps. In the first step, a depletion calculation is performed with Serpent2 [6] to get the isotopic content of the spent fuel. In the second step, the neutron transport and detection is simulated in MCNP6 [7].

Simulations have been performed for 1040 PWR spent fuel assemblies, covering a range of values of IE, BU and CT. IE ranges from 2-5 % atomic weight in steps of 0.25 % (corresponding to a range of 1.98 to 4.94 % in mass weight), and BU ranges between 15-60 GWd/tU in

steps of 5 GWd/tU up to 40 GWd/tU and then in two more steps of 10 GWd/tU. CT ranges between 5-70 y, with smaller steps for shorter cooling times (5 y, 7.5 y, 10 y, 12.5 y, 15 y, 20 y, 30 y, 40 y, 55 y and 70 y). The choice of a grid with an uneven sampling of BU and CT space is made to more accurately capture the variation of τ with these variables, with a smaller grid spacing where τ changes more rapidly.

2.1 Burnup calculation

The burnup, or depletion, calculation is performed in Serpent2 in criticality source mode, in an infinite 2D lattice. The geometry consists of one pin surrounded by water, with reflective boundary conditions. The pin radius is 0.41 cm, the inner cladding radius 0.42 cm, the outer cladding radius 0.48 cm and the pitch 1.26 cm.

The fuel cycles are defined as cycles of 365 days of irradiation at constant power density, resulting in a burnup of 10 GWd/tU per cycle, followed by a down-time of 30 days. The length of the last cycle is adjusted to give the desired burnup, and the desired cooling time is then calculated with the radioactive decay of the spent fuel.

The simulated spent fuel assemblies resulting from this depletion calculation are ideal in several respects: the assembly is uniform, all pins have identical properties; and all assemblies follow idealized cycles (while commercial assemblies might *e.g.* spend a cycle outside the reactor).

2.2 DDSI physics and modelling

The DDSI instrument consists of 56 ^{3}He tubes in four detector pods surrounding the fuel assembly, as described in [1]. The instrument detects neutrons emitted from the spent nuclear fuel, and can be used to calculate the early die-away time τ.

The detected neutrons follow the Rossi-alpha distribution (shown in figure 1). This distribution describes the time difference between detected neutrons, and the non-flat distribution can be explained by the correlation between detected neutrons from the same fission or fission chain. There are in fact two components that describe the neutron correlation, a fast and a slow component, and both are exponential in nature. The fast component corresponds to neutrons from the same fission event or from a fast fission chain, but since the instrument is not capable of resolving this time scale, the decay time of this component instead depends on the instrument geometry and the thermalization of the neutrons before detection. The slow component corresponds to neutrons from a thermal fission chain, i.e. where the neutron thermalizes before inducing a new fission.

The early die-way time results from an interplay between the two components, and has been shown [3-5] to be proportional to the multiplication of the fuel assembly. τ measures how long the neutron population survives in the spent fuel and a larger τ -value shows that the neutrons die-away more slowly. Fissile material therefore increases τ, while neutron poisons decrease it, and the value for each spent fuel assembly is a result of the interplay between these two types of materials.

In MCNP6, the DDSI instrument is modelled surrounding PWR 17x17 spent fuel assemblies, all submerged in water. The fuel pins in the assembly have the geometry described earlier, and the material composition is taken from the output of the Serpent2 simulation. The source term is defined as a spontaneous fission source, and it is distributed evenly in all the fuel rods. The source is restricted to 145 cm of axial length, centred on the DDSI instrument, as a means to speed up the simulation while retaining most of the signal (for details see [8]). The F8 coincidence capture tallies are used to calculate the Rossi-alpha distribution of real coincidences, similarly as in [1]. The Rossi-alpha distribution is simulated from 0 to 200 μs, and τ is calculated from an exponential fit over the range 4-52 μs (including statistical errors).

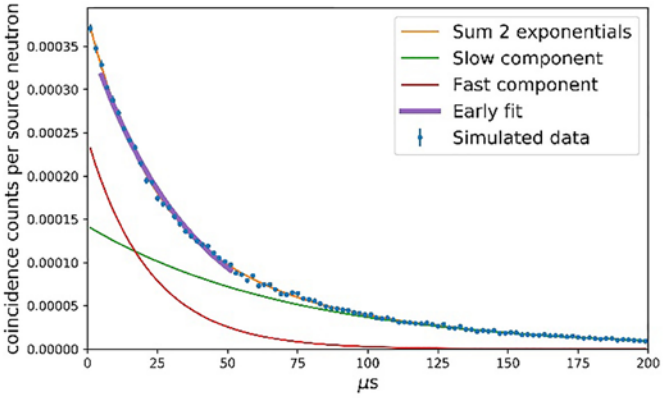

Figure 1: Rossi-alpha distribution for real coincident neutrons as simulated with MCNP6. The simulated spent fuel assembly has IE=3.5 %, BU=43 GWd/tU and CT=59 y, and τ= 37.0 ± 0.4 μs.

3. Parametrization of τ

Intuitively, since the early die-away time is proportional to multiplication, we expect it to decrease with BU (less fissile material and more neutron absorbers are present) and to increase with IE (more fissile material is present). The CT dependence is not so intuitive, most of the fissile material will not depend on CT, although ^{241}Pu does. Figures 2-4 show how τ depends on IE, BU and CT for a part of the data. The dependence for the whole dataset is smooth, and an interpolation between the shown data points can be made.

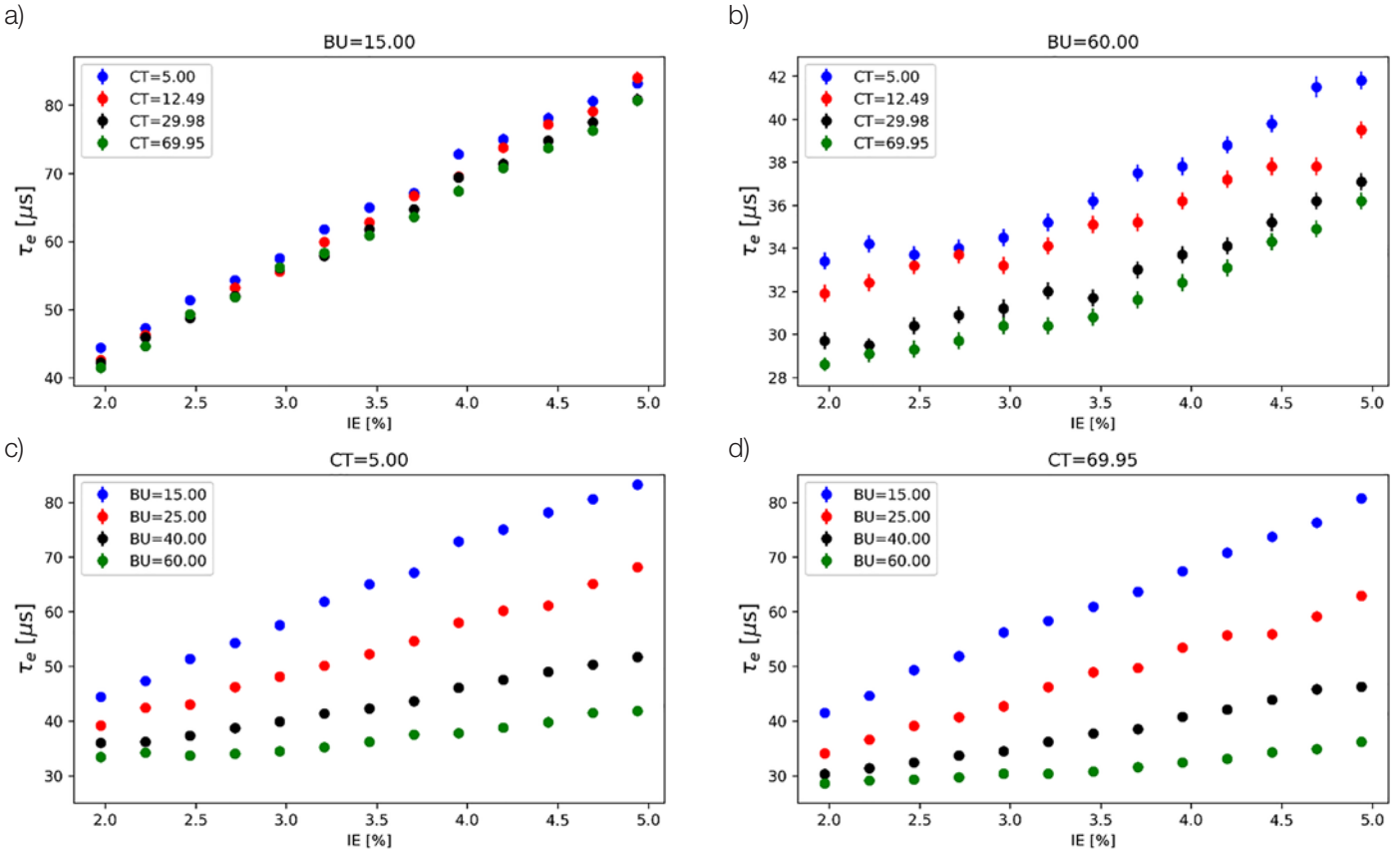

Figure 2: The τ dependence on IE, for low BU (a), high BU (b), low CT (c) and high CT (d). In the top figures, the colors indicate different CT, for the bottom figures it indicates different BU. For a more understandable figure, all simulated data points are not shown.

As can be seen from figures 2a-2d, there is a strong dependence of τ on IE. As expected, τ increases with increasing IE. Figures 2a-2b show that the IE dependence does not depend on CT, since the data sets corresponding to different CT are only separated by a constant offset depending on CT. Figures 2c-2d however show a noticeable effect of BU on the IE dependence, with an increasing slope for lower BU-values.

Similar conclusions can be drawn from figure 3. Figures 3a-3b show a similar shape of the τ-dependence

on BU independent of CT (only the constant offset is different), while figures 3c-3d show a dependence on IE where different IE-values give different slopes to the τ-dependence on BU.

Figure 4 shows that the CT-dependence can be described with an exponentially decreasing function, with figures 4a-4b showing that IE only affects a constant offset and not the exponential itself, and figures 4c-4d show the same but for BU. The different scales of the y-axis make it difficult to compare different subplots with each other, but one can note this effect also by comparing the different colors in each subfigure (they colored data sets only vary by a constant offset). This implies that the CT dependence, described by an exponential function, is independent of IE and BU except for a constant offset. Since the IE and BU dependencies are interconnected, it is more difficult to assess what functional form to use in order to describe them. However, the figures qualitatively tell us that τ increases with IE, with a steeper slope for low BU (e.g. figure 2c); and τ decreases with BU, with a slope that increases with higher IE and flattens out with BU (eg figure 3c).

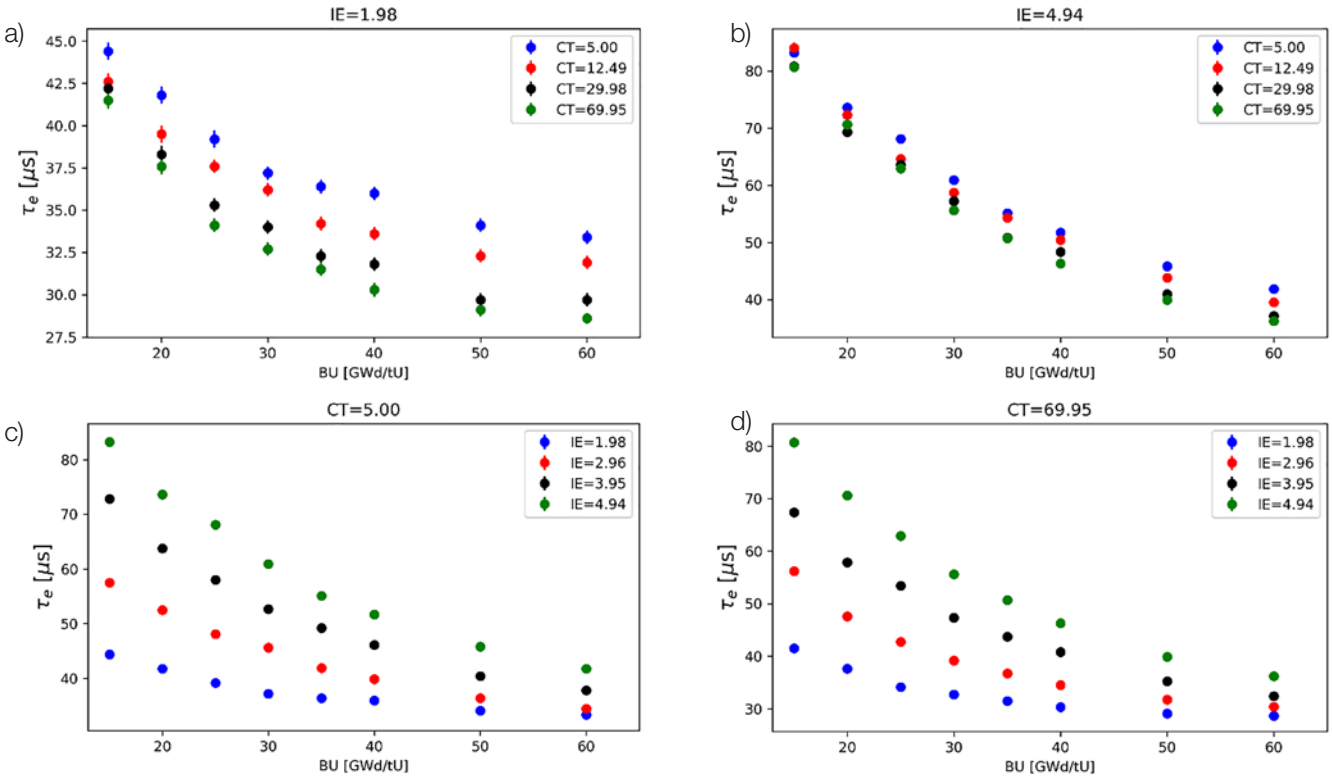

Figure 3: The τ dependence on BU, for low IE (a), high IE (b), low CT (c) and high CT (d). For the top figures, the colors indicate different CT, for the bottom figure it indicates different IE. For a more understandable figure, all simulated data points are not shown.

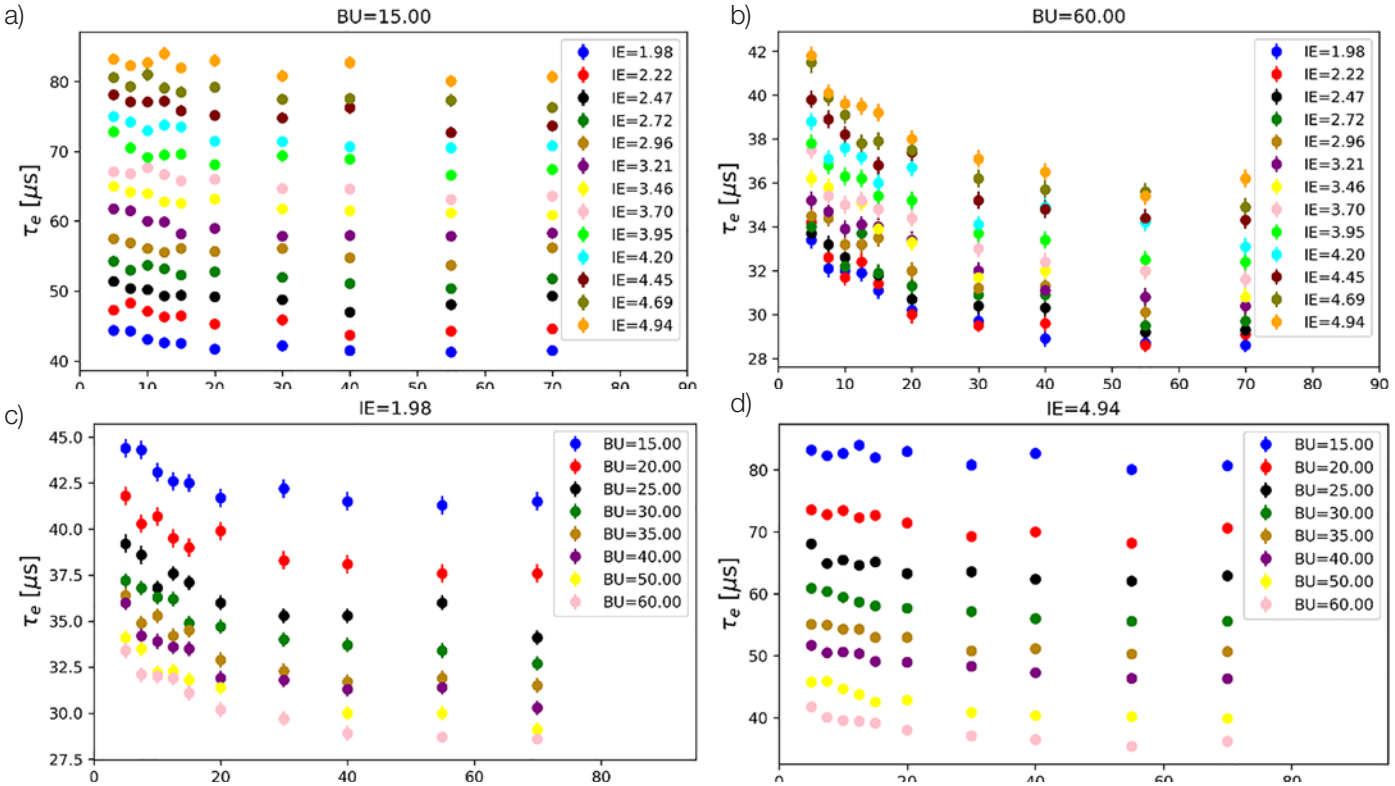

Figure 4: The τ dependence on CT, for low BU (a), high BU (b), low IE (c) and high IE (d). For the top figures, the colors indicate different IE, for the bottom figure the colors indicates different BU.

3.1 Physical considerations

As mentioned above, the early die-away time depends on the quantity of fissile material and neutron absorbers (such as some fission products) in the fuel. To understand which isotopes that are most important when determining τ, we have investigated three quantities in eight example fuels: i) the neutron absorption rate, ii) the neutron induced fission rate and iii) the rate of neutrons produced from fission. The eight example fuels have low and high CT, low and high BU and low and high IE. The respective rates were calculated using the MCNP6 F4 neutron flux tally score, multiplied with the relevant cross-sections. The isotopes where then ranked according to the absolute value of their net neutron emission rate, defined as the difference between the neutron emission rate from fission and the total neutron absorption, where total neutron absorption also includes neutrons lost to fission.

Looking at the top six isotopes for each of the eight example fuels, we find that the sixth isotope always has a net neutron emission which is at least one order of magnitude smaller than the first isotope. Table 1 shows the six top ranked isotopes for one of the eight fuels.

Isotope	Net neutron emission [au]
^{239}Pu	7.8
^{235}U	4.4
^{238}U	-4.2
^{241}Pu	2.4
^{240}Pu	-2.0
^{143}Nd	-0.51

Table 1: Net neutron emissions for an example fuel with IE=4.9%, BU=60 GWd/tU and CT=5y.

To reach a reduction in net neutron emission of two orders of magnitude, it was sometimes necessary to consider 30 ranked isotopes. In qualitatively understanding the impact of the different isotopes on τ, we focus here on eight isotopes that appear at least once in the top five list for the eight fuels: ^{239}Pu, ^{240}Pu, ^{241}Pu, ^{241}Am, ^{235}U, ^{238}U, ^{155}Gd and ^{149}Sm. The top 3 list is often consisting of ^{239}Pu, ^{235}U and ^{238}U. The following subsections give some insight into the mechanism governing τ and its dependence on IE, BU and CT. A more quantitative understanding is beyond the scope of this paper.

3.1.1 CT dependence of τ

From the list of isotopes above, the one isotope with a half-life likely to have a visible effect in the range of CT=5-70 y is ^{241}Pu ($t_{½}$ = 14.3 y). This isotope mainly β^--decays to ^{241}Am. While ^{241}Pu is fissile and has a positive contribution to the early die-away time (more ^{241}Pu gives a larger τ), ^{241}Am absorbs neutrons and has a low probability of fissioning, and thus has a negative contribution to τ. From these considerations, one would expect τ to follow an exponential decay law with CT, with a mean lifetime (the inverse of the exponential decay constant λ) smaller than that of ^{241}Pu, since the decay of ^{241}Pu creates ^{241}Am which lowers τ even more. This is indeed the result found in the study; the mean lifetime of ^{241}Pu is 20.6 y, and the mean lifetime obtained for τ in the fit in section 3.2.1 is 15.8 y (parameter *b* in table 3).

3.1.2 BU and IE dependence of τ

Since higher BU means that more fissile ^{235}U nuclei have been split, τ is expected to decrease with BU. The buildup of other fissile isotopes should offset this and slow down the decrease, while production of neutron poisons would speed up the decrease. Studying how the ^{235}U concentration changes as a function of burnup, we note that the rate of decrease of the ^{235}U concentration depends on the IE, with higher IE resulting in a sharper decrease of the ^{235}U concentration with increasing BU.

Figure 5 shows how the total fissile concentration (i.e. ^{235}U, ^{239}Pu and ^{241}Pu) changes with BU and IE. This dependence is very similar to the dependences observed for only ^{235}U, and this isotope is hence assumed to dominate the dependence. The dependences in figure 5 are qualitatively

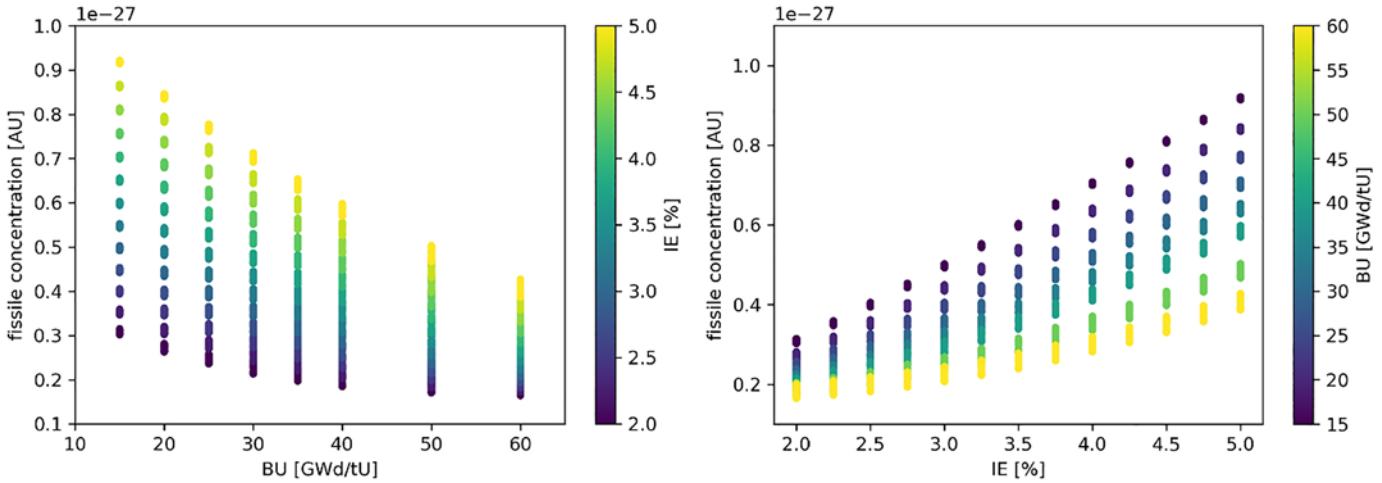

Figure 5: The concentration of fissile isotopes vs BU (left) and IE (right), colored with the IE (left) and BU (right).

very similar to the τ-dependence on these variables, so the contribution from ^{235}U seems to be the most important one. Higher IE, meaning more ^{235}U and less ^{238}U, is expected to give larger values of τ, as is also seen in figure 2. As BU increases, the fuel composition becomes more complex and varied and the increase of τ with IE slows down.

3.2 Fitting functions

Since the τ-dependence on CT seems to be independent of BU and IE, this was investigated first. The function describing the dependence of τ on CT was chosen to be an exponential function of the form

$$\tau = a \cdot e^{-\frac{CT}{b}} + c \quad (1)$$

where *a*, *b* and *c* are the fitting parameters. The choice of the exponential function is explained in section 3.1.1. One exponential function (each generating unique *a*, *b* and *c* parameter values) was fitted to each group of data points with one combination of IE and BU, e.g. each group with the same color in one subplot of figure 4. The fit parameters *a*, *b* and *c* are then analyzed with respect to their dependence on IE and BU. The dependences of the *a* and *c* parameters on BU and IE can be seen in figure 6; the dependence of the *b* parameter looks similar to the *a* dependence and is hence not shown.

Despite rather large statistical fluctuations in figure 6 (the error bars represent the statistical uncertainties in the fit), both the *a* and *b* parameters have been found to be consistent with a constant value. This means that these two parameters can be considered to be independent of IE and BU. The *c* parameter however displays the same trend as τ does for a fixed CT, also indicating that the BU and IE dependence of τ is captured by the *c*-parameter and not by the *a* or *b* parameters. With the ultimate goal of finding a function that describes how τ varies with IE, BU and CT, equation 1 was accordingly chosen with the *a* and *b* parameters constant for the whole range of IE and BU values, but with the *c* parameter replaced by a function that better captures the IE and BU dependences.

In the determination of the second function (capturing the dependence of the *c* parameter on BU and IE), a fit of equation 1 was performed to fix the *a* and *b* constants while allowing the *c* parameter to vary with BU and IE. Accordingly, a different *c* parameter value was obtained for each value of IE and BU.

Determining then the BU dependence first, and to avoid an unphysical increase of τ with BU values outside the fitting range, an exponential fit (Equation 2) was tried

$$c = a_1 \cdot e^{-\frac{BU}{b_1}} + c_1 \quad (2)$$

where a_1, b_1 and c_1 are the fit parameters that vary with IE. Since each fit, corresponding to one IE value, is associated with a unique determination of the parameters a_1, b_1 and c_1, a function can be used to describe how each parameter varies with IE. This function can be described by either a linear, quadratic or constant polynomial of IE. Figure 7 shows the variation of the parameter values with IE, together with a linear fit.

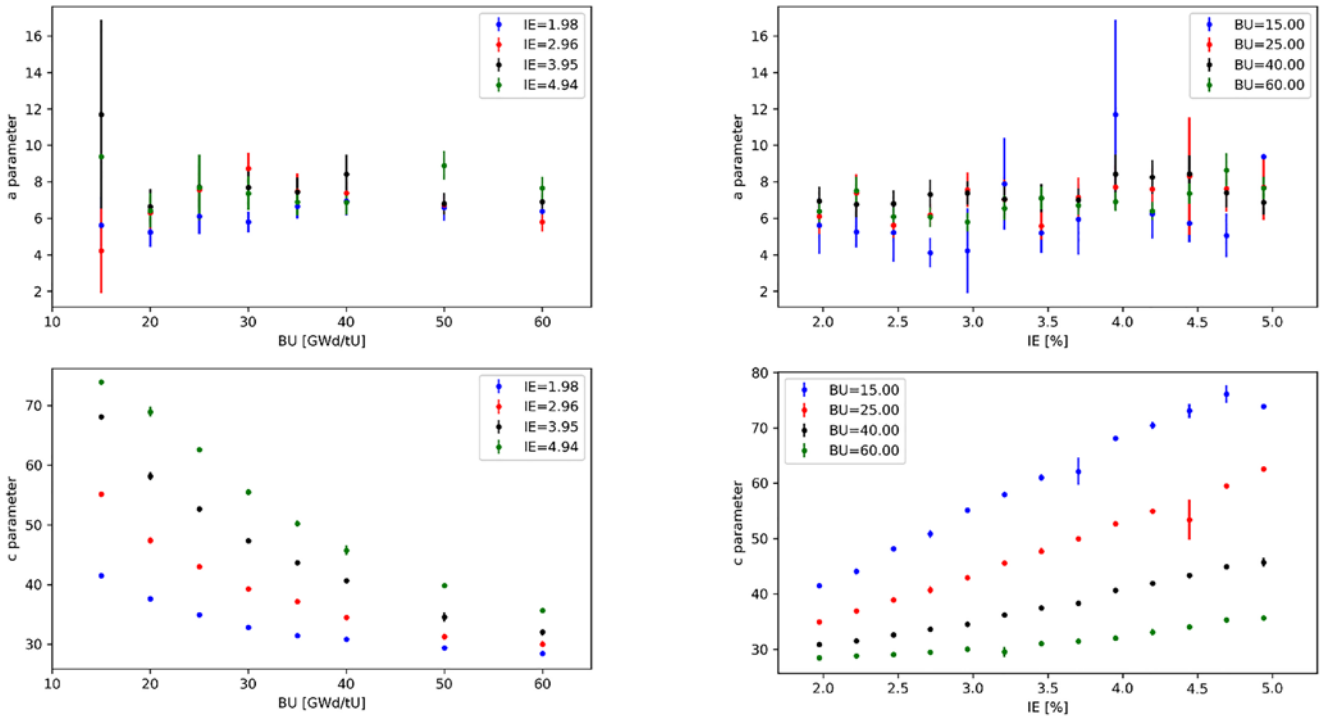

Figure 6: The *a* (upper row) and *c* (lower row) parameters resulting from an exponential fit of τ to CT, shown as a function of BU (left) and IE (right). The data points corresponding to BU=15 GWd/tU and IE=4,94% are plotted without error bars, since the error associated these points is so large that they obscure all other trends. For a more understandable figure, all simulated data points are not shown.

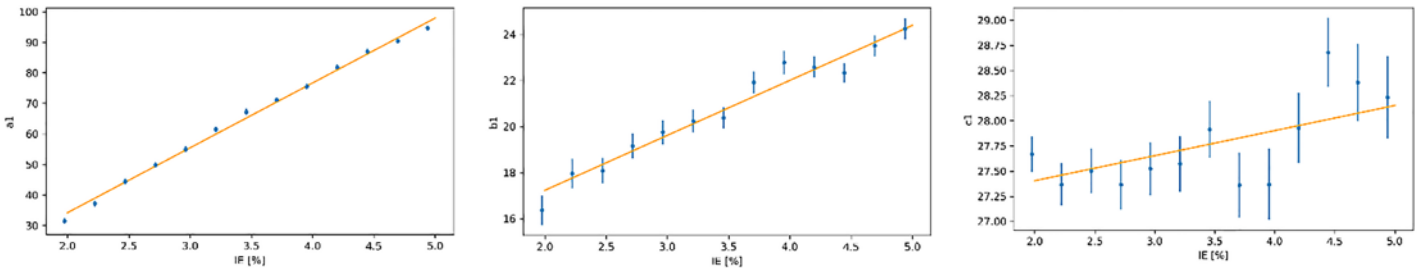

Figure 7: The dependence of the parameters a_1, b_1 and c_1 of the BU fit (equation 2) on IE. The fitted function is linear in all three cases, although table 2 shows that this does not always give the best fit.

Table 2 shows the resulting χ^2 and χ^2 probability values for different functions describing the variation of the a_1, b_1 and c_1 parameters with IE. Table 2 tells us that the a_1 parameter is best described by a function that depends quadratically on IE, the b_1-parameter is best described by a linear function of IE (although the quadratic function is almost equally good), and that the c_1 parameter is best described by a quadratic function (but a linear function is still relevant to try in a global fit).

Parameter	Fit type	χ^2	χ^2 probability
a_1	Linear	25.7	0.007
	Quadratic	5.2	0.88
b_1	Linear	10.7	0.45
	Quadratic	8.6	0.57
c_1	Linear	12.6	0.32
	Quadratic	8.0	0.62
	Constant	21.3	0.04

Table 2: Fit statistics for the BU parameters a_1, b_1 and c_1 as functions of IE.

3.2.1 Global fit

Following the considerations above, several functions were tried in order to find a suitable function for a global fit, that simultaneously describes the dependence of τ on CT, BU and IE. All the functions which were tried, make use of equation 1 but with parameter c replaced by a function C, as shown in equation 3:

$$\tau = a \cdot e^{-\frac{CT}{b}} + C \tag{3}$$

Many different functions C were tried and assessed, the best function as determined by the resulting χ^2 value is shown in equations 4-7

$$C = c' \cdot e^{-\frac{BU}{d}} + e \tag{4}$$

$$c' = \left(c_2 \cdot IE^2 + c_1 \cdot IE + c_0\right) \tag{5}$$

$$d = \left(d_2 \cdot IE^2 + d_1 \cdot IE + d_0\right) \tag{6}$$

$$e = \left(e_2 \cdot IE^2 + e_1 \cdot IE + e_0\right) \tag{7}$$

The resulting parameter values are shown in table 3. This fit has $\chi^2 = 1245$ and χ^2 probability $3.9 \cdot 10^{-6}$. The errors are probably underestimated, leading to this large value of χ^2, and a better error estimate is under consideration.

Figure 8 shows the τ value determined using the parametrization versus the τ value determined using the MCNP simulations, together with the line representing a perfect fit. As can be understood, the global parametrization function seems to work quite well.

Parameter	Value
a	6.87(8)
b	15.8(4)
c0	-28(3)
c1	33(2)
c2	-1.8(2)
d0	11(1)
d1	3.3(7)
d2	-0.14(10)
e0	28.2(6)
e1	-0.7(4)
e2	0.14(7)

Table 3: Fit parameters determined for the best global fit.

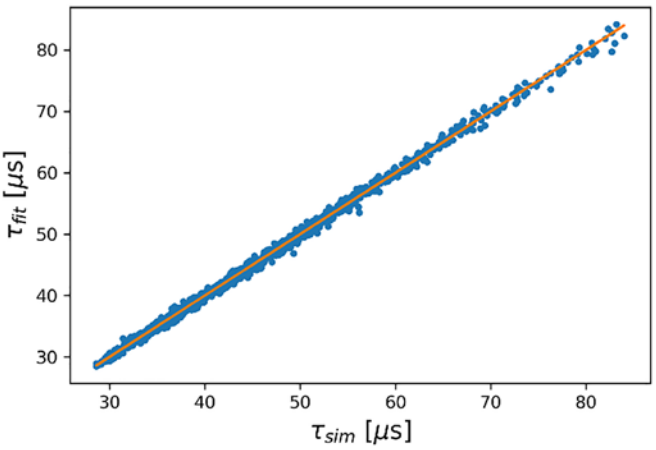

Figure 8: The τ values determined from the parametrization versus those obtained from a full-scale MCNP6 modelling together with a line indicating a perfect match.

4. Test of parametrization

The parametrization has been tested on a separate set of modelled data. The data set comprises 980 simulated PWR fuels, with depletion calculations done using Serpent2 as described in section 2. However, the ranges of IE, BU and CT were slightly different from the fuels described earlier. IE ranged from 2-5% atomic weight in steps of 0.5%, while BU and CT were randomly selected with a uniform probability in the intervals 15-50 GWd/tU and 5-70 y, respectively. Figure 9 shows the early die-away time τ determined using the parametrization versus determination using MCNP, as well as the normalized residuals $r_n = \frac{\tau_{fit} - \tau_{sim}}{\sigma_{\tau_{sim}}}$, centered around zero.

The root mean squared error (RMSE) is 0.57 μs, χ^2 = 1131 and the χ^2 probability $5.4 \cdot 10^{-4}$. As previously mentioned, the errors are probably underestimated, leading to a larger value of χ^2 than is to be expected, but this remains to be investigated.

5. Conclusion and Outlook

This paper describes a way to estimate the early die-away time τ from the DDSI prototype instrument, as a way to avoid the computationally demanding MCNP simulations that are usually performed. This can be specifically useful when die-away times for large number of fuel assemblies are required, such as in the case of training machine learning models.

Our work shows that in the case of modelled PWR 17x17 fuel assemblies, the CT dependence of the early die-away time can be decoupled from the BU and IE dependencies. The research also suggested that the CT dependence of τ follows an exponential decay. In this work it was decided to, in the second step, describe the BU dependence and thirdly the IE dependence. The reverse order was tried, although the results are not shown in this paper, and the results were similar to those obtained here but not as good. The BU dependence could be best described using another exponential decay, although other functions with a similar fall-off were found to also work well. The IE-dependence was finally captured using functions with a quadratic dependence on this parameter.

The die-away times estimated using the resulting parametrization function were compared to the accurate estimations using MCNP6 modelling and a fit to the Rossi-alpha distribution, and the agreement was shown to be very good, also for the case of a new data set of modelled fuel assemblies with a slightly different set of fuel parameters (within the same range as the first one). As an important next step, an experimental validation of this parametrization is planned, since the ability of the parametrizing function to estimate the DDSI die-away time for commercial reactor fuel might be significantly influenced by a deviation of burnup, initial enrichment and cooling time from the assumed ideal case. Furthermore, it is important to study to what extent the parametrization function also correctly estimates the die-away time for other fuel types or designs.

6. Acknowledgements

We would like to acknowledge the financial support from the Swedish Radiation Safety Authority under contracts SSM2016-661, SSM2015-4125 and SSM2016-4600.

The authors would also like to thank Dr. Alexis Trahan at Los Alamos National Laboratory for her kind assistance with respect to DDSI modelling.

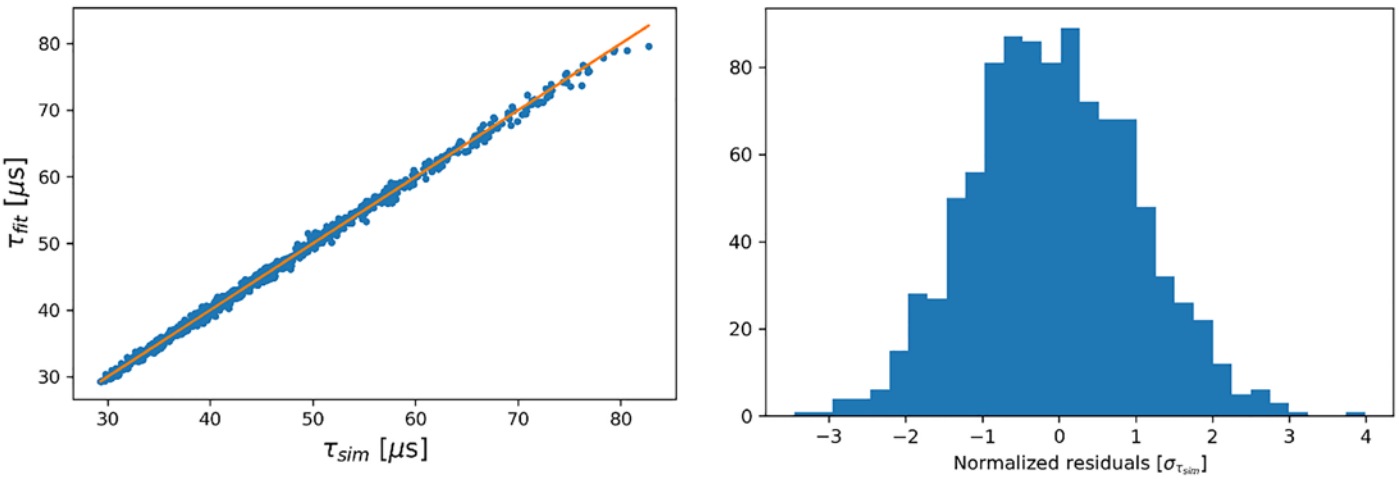

Figure 9: The simulated and calculated values of τ for the test data fall close to the line indicating a perfect match (left). The normalized residuals are shown in the right figure.

7. References

[1] A. Trahan. “Utilization of the Differential Die-Away Self-Interrogation Technique for Characterization and Verification of Spent Nuclear Fuel”. PhD thesis. University of Michigan, 2016.

[2] M. A. Humphrey, S. T. Tobin, and K. D. Veal. “The Next Generation Safeguards Initiative’s Spent Fuel Nondestructive Assay Project”. In: Journal of Nuclear Material Management 40 (2012), pp. 6-11.

[3] A. Trahan, G. McMath, P. Mendoza, H. Trellue, U. Backstrom, and A. Sjöland. “Preliminary Results from the Spent Nuclear Fuel Assembly Field Trials with the Differential Die-Away Self-Interrogation Instrument”. In: Proceedings of the Institute of Nuclear Materials Management 59th Annual Meeting, July 22-26, Baltimore, Maryland. Institute of Nuclear Materials Management. 2018.

[4] A. C. Kaplan, V. Henzl, H. O. Menlove, M. T. Swinhoe, A. P. Belian, M. Flaska, and S. A. Pozzi. “Determination of spent nuclear fuel assembly multiplication with the differential die-away self-interrogation instrument”. In: Nuclear Instruments and Methods in Physics Research Section A: Accelerators, Spectrometers, Detectors and Associated Equipment 757 (2014), pp. 20-27.

[5] A. C. Trahan, A. P. Belian, M. T. Swinhoe, H. O. Menlove, M. Flaska, and S. A. Pozzi. “Fresh Fuel Measurements with the Differential Die-Away Self-Interrogation Instrument”. In: IEEE Transactions on Nuclear Science 64.7 (2017), pp. 1664-1669.

[6] J. Leppänen, M. Pusa, T. Viitanen, V. Valtavirta, and T. Kaltiaisenaho. “The Serpent Monte Carlo code: Status, development and applications in 2013”. In: Annals of Nuclear Energy 82 (2015), pp. 142-150.

[7] T. Goorley et al. “Initial MCNP6 Release Overview”. In: Nuclear Technology 180.3 (2012), pp. 298-315.

[8] L. Caldeira Balkeståhl, Z. Elter, S. Grape, and C. Hellesen. “MCNP simulations of prototype DDSI detector”. In: Proceedings of the International Workshop on Numerical Modelling of NDA Instrumentation and Methods for Nuclear Safeguards (NM-NDA-IMNS18). ESARDA. 2018.